

I-	Legends of supplemental Figures 1-5	2
II-	Supplemental Figures 1-5	4
III-	Supplemental Tables 1-3	9
IV-	Supplemental Methods	12
V-	References	19

I- Legends of supplemental Figures 1-5

Supplemental Figure 1: X-Gal staining in *ROSA26^{+/-},Myo15-cre^{+/-}* mice, and anti-clarin-1 antibodies

(A) X-Gal staining in *ROSA26^{+/-},Myo15-cre^{+/-}* mice. To test possible expression in the cochlear ganglion, the cre-driven *lacZ* expression was studied in *ROSA26^{+/-},Myo15-cre^{+/-}* mice by X-Gal histochemistry on postnatal day 15 (P15). *LacZ* expression is detected in the inner (IHCs) and outer (OHCs) hair cells, but not in the primary auditory neurons (cochlear ganglion neurons).

(B) DPOAE amplitudes in control and *Clrn1^{ex4fl/fl},Myo15-cre^{+/-}* mice. For both 10 kHz and 15 kHz (f_2 values, with $f_2/f_1 = 1.2$) dual tone stimuli (65 dB SPL), DPOAE amplitudes in *Clrn1^{ex4fl/fl},Myo15-cre^{+/-}* mice (red), within the normal range on P15-P20, are significantly lower in control mice (grey) on P21-P28 and P30-P60. (ns) and (***) denote statistically not significant ($P > 0.05$), and significant ($P < 0.001$) difference, respectively (two-way ANOVA).

Supplemental Figure 2: Abnormal shapes of the hair bundles in *Clrn1^{ex4-/-}* mice, but not in *Clrn1^{ex4fl/fl},Myo15-cre^{+/-}* mice

(A-D) Top views of cochlear whole-mounts from *Clrn1^{ex4-/-}*, *Clrn1^{ex4fl/fl},Myo15-cre^{+/-}* and control mice (confocal and scanning electron microscopy). (A) Instead of the normal V-shaped hair bundles in control mice (left panel), various abnormal shapes are observed in the OHC hair bundles of *Clrn1^{ex4-/-}* P5 mice (right panel). F-actin labeling with TRITC-phalloidin (red) was used to visualize the stereocilia. Representative scanning electron micrographs of OHC hair bundles from P12 *Clrn1^{ex4-/-}* mice displaying shapes similar to those of the immunostained (harmonin b, green) hair bundles are presented. (B) Altered shape of the hair bundles and regression of the short row stereocilia in OHCs of *Clrn1^{ex4-/-}* mice. Unlike in the P12 control OHC hair bundle (left), almost all the stereocilia in the hair bundle short row (artificially colored in red) of OHCs in *Clrn1^{ex4-/-}* mice have disappeared. (C) On P15 and P20 in *Clrn1^{ex4fl/fl},Myo15-cre^{+/-}* mice, the shapes of the OHCs hair bundles are well preserved, with persistence of all three rows of stereocilia at these stages. (D) The typical targeting of USH1 proteins (myosin VIIa, harmonin b, cadherin-23, & protocadherin-15) in the apical region of F-actin-labeled stereocilia (red) is preserved in P12 *Clrn1^{ex4fl/fl},Myo15-cre^{+/-}* mice. Bars: 1 μ m.

Supplemental Figure 3: Progressive loss of stereocilia in the auditory hair bundles in *Clrn1^{ex4fl/fl},Myo15-cre^{+/-}* mice.

(A) Representative examples of OHC and IHC hair bundles between P20 and P60 illustrating the progressive loss of stereocilia in the short row of the hair bundle in *Clrn1^{ex4fl/fl},Myo15-cre^{+/-}* mice,

after P30. The boxed area in the right panel is used in Figure 2C. The shape of the hair bundles is preserved, but many stereocilia in the short stereocilia row of both OHCs and IHCs display reduced lengths, and some stereocilia have even disappeared (arrows). (B) On P120, the stereocilia of the short row have disappeared and many OHCs hair bundles are lost. (C) Comparative evolution with age of click ABR thresholds. Significant hearing protection was observed in the injected ears of *Clrn1^{ex4fl/fl},Myo15-cre^{+/-}* mice at all analyzed stages, as compared with age-matched non injected ears. (D) The progressive loss of the hair bundles in *Clrn1^{ex4fl/fl},Myo15-cre^{+/-}* mice is delayed upon viral injection of AAV2/8-*Clrn1* in the inner ear. The preserved tenting at the extreme tip of stereocilia in the short and middle rows of some IHC hair bundles is indicative of persisting tension due to mechano-electrical transduction activity. Bars: 1 μ m.

Supplemental Figure 4: Clarin-1 expression and test of anti-clarin-1 antibodies.

(A) Immunoblot analysis of the anti-clarin-1 polyclonal antibody. The stained gel with Coomassie blue shows the positions of the GST-tagged Clrn1-N fusion proteins (136 aa containing the two first transmembrane domains TM1 and TM2). In the two right panels, mcherry-clarin-1 is detected using either the anti-clarin-1 or the anti-RFP (Rockland, N° 600-401-379) antibodies. (B,C) Transfected HeLa cells (ATCC) producing mCherry-tagged clarin-1 (red) were labeled by the homemade anti-clarin-1 antibodies (green). The anti-clarin-1 immunostaining and mCherry staining strictly overlap (yellow), including at the plasma membrane (arrows in B). (C) Conversely, neither of the Novus (N° 42720002)- or Sigma (HPA054636)-commercial anti-clarin-1 antibodies did label the over-expressed mCherry-tagged clarin-1. Bars: 10 μ m.

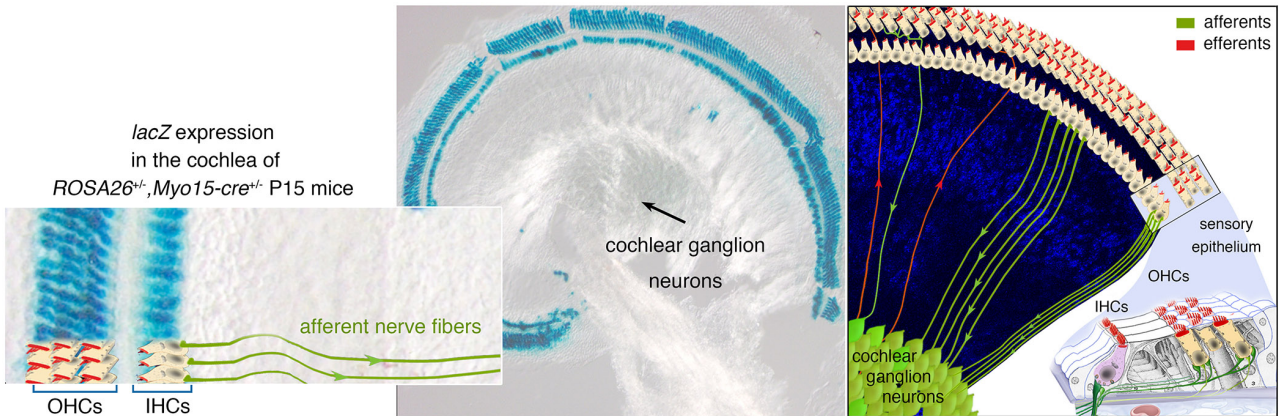
Supplemental Figure 5: Clarin-1 is required for the proper organization of the postsynaptic AMPA receptors GluA2/3 in *Clrn1^{ex4fl/fl},Myo15-cre^{+/-}* mice.

(A,B) Whole mounts of organs of Corti of control and *Clrn1^{ex4fl/fl},Myo15-cre^{+/-}* P18 (A) and P20 (B) mice double-immunolabeled for ribeye and GluA2 glutamate receptors. Control IHCs display restricted and juxtaposed ribeye- and GluA2-immunolabeled patches in their active zones. In contrast, a postsynaptic expansion of the GluA2-immunoreactive domains is observed in the afferent terminals facing the IHC ribbons of *Clrn1^{ex4fl/fl},Myo15-cre^{+/-}* mice. The expansion of the GluA2/3 glutamate receptors was observed in all analyzed *Clrn1^{ex4fl/fl},Myo15-cre^{+/-}* P18 and P20 mice, but its extent varies within the same cochlea and among *Clrn1^{ex4fl/fl},Myo15-cre^{+/-}* mice. Bars: 1 μ m.

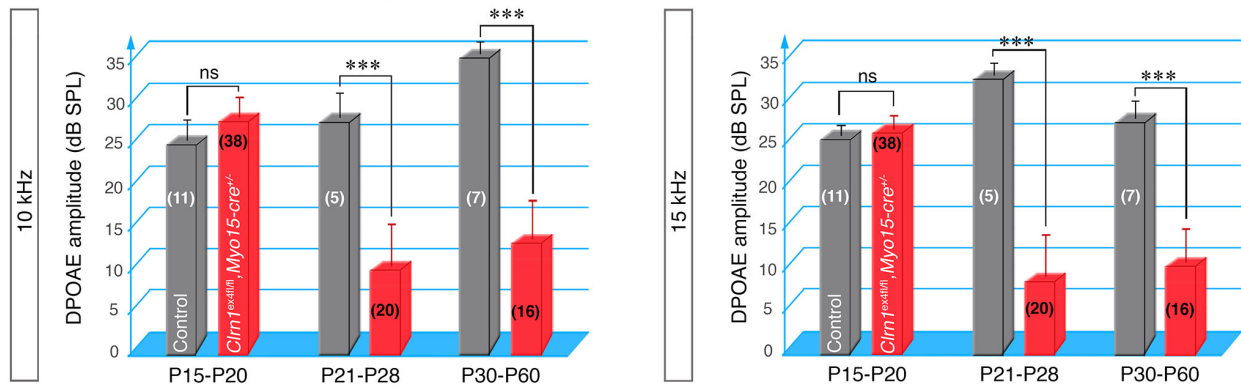
II- Supplemental Figures 1-5

Supplemental Figure 1: X-Gal staining in *ROSA26^{+/+}, Myo15-cre^{+/-}* mice, and anti-clarin-1 antibodies

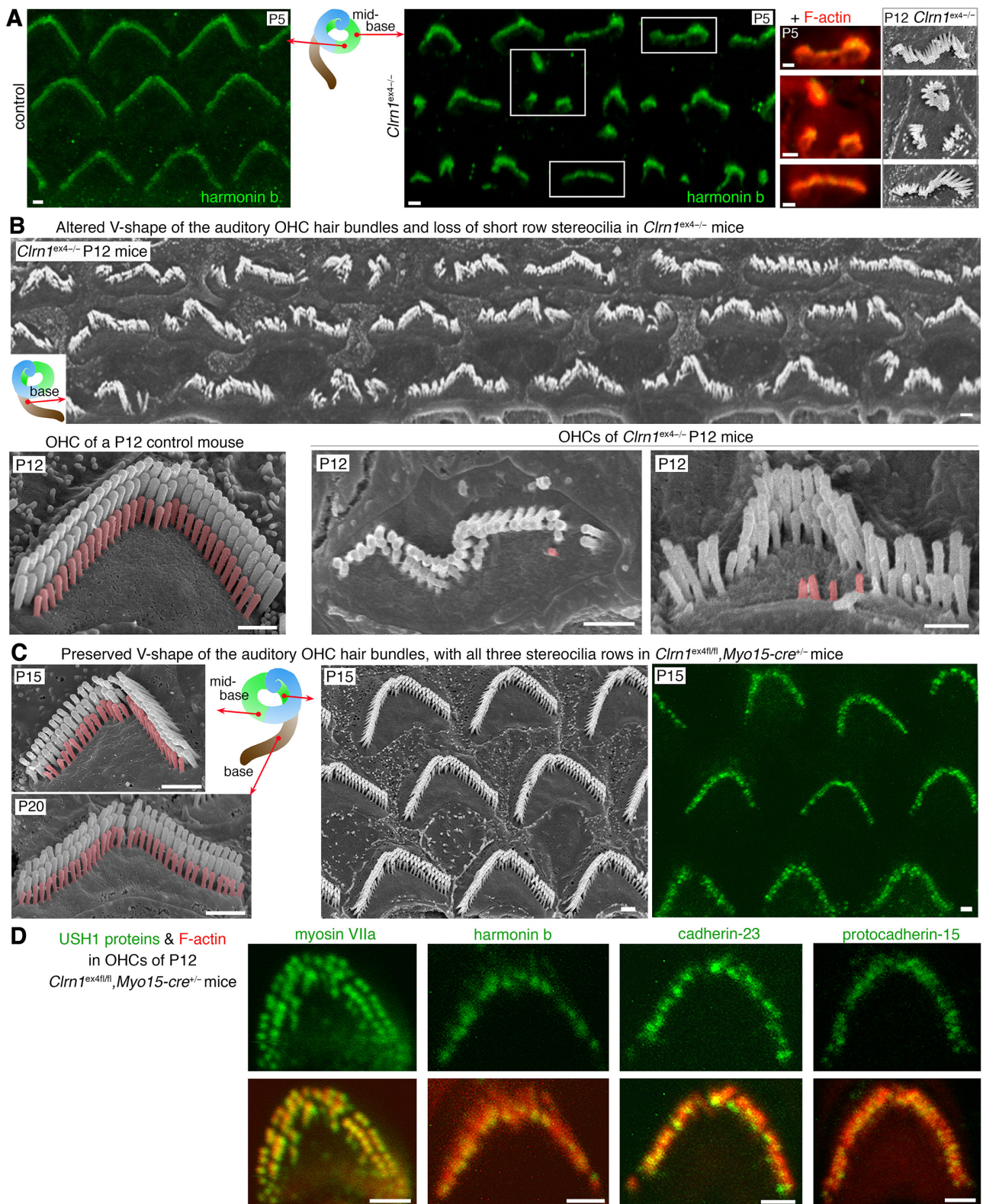
A The cre gene driven by the *Myo15* promoter is expressed in the hair cells, but not in primary auditory neurons



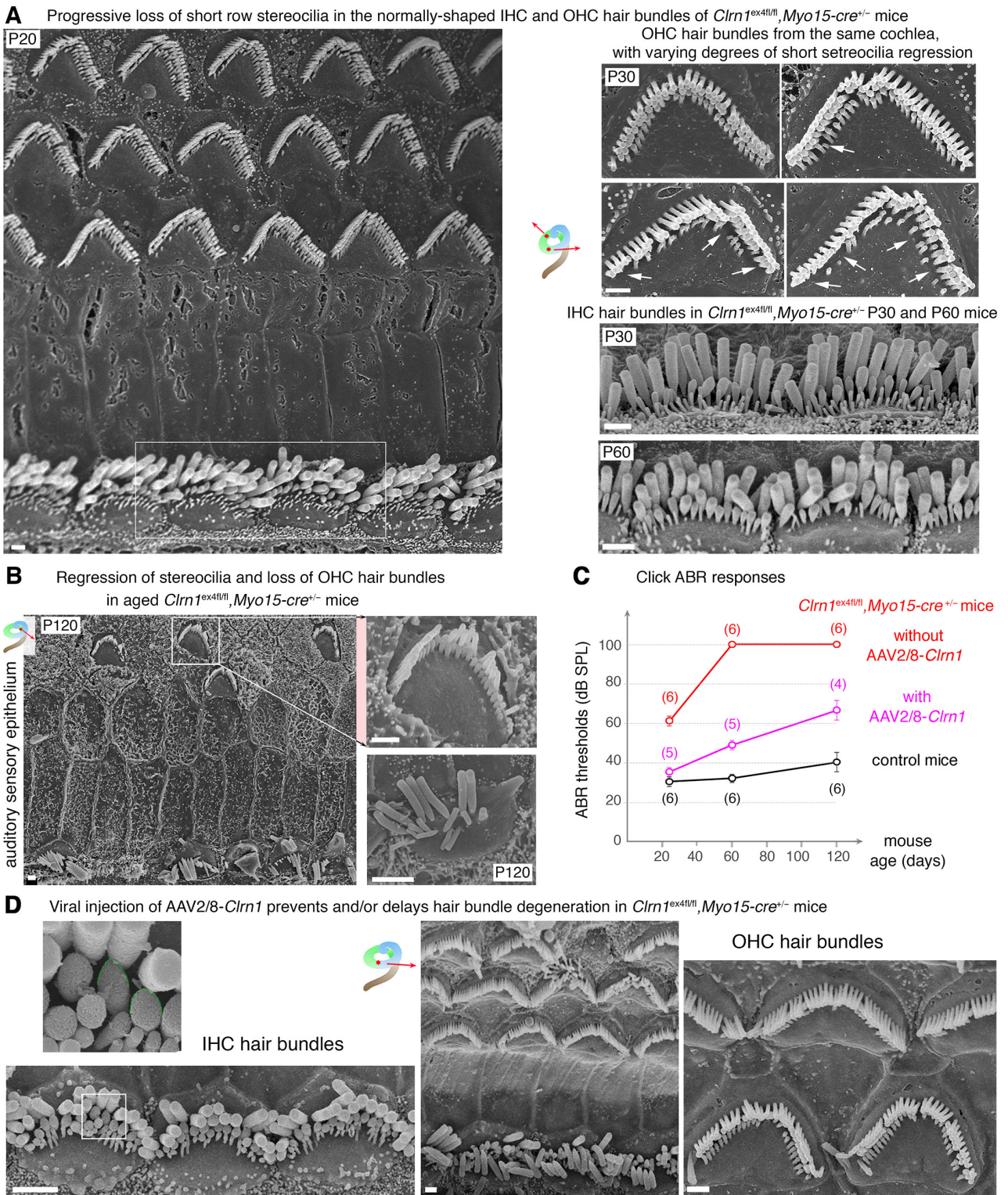
B DPOAE amplitudes in *Clrn1^{ex41fl/fl}, Myo15-cre^{+/-}* mice



Supplemental Figure 2: Abnormal shapes of the hair bundles in *Clrn1*^{ex4-/-} mice, but not in *Clrn1*^{ex4fl/fl},*Myo15-cre*^{+/-} mice

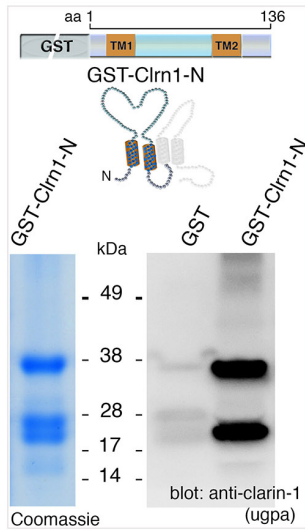


Supplemental Figure 3: Progressive loss of stereocilia in the auditory hair bundles in *Clnn1^{ex4fl/fl}, Myo15-cre^{+/-}* mice.

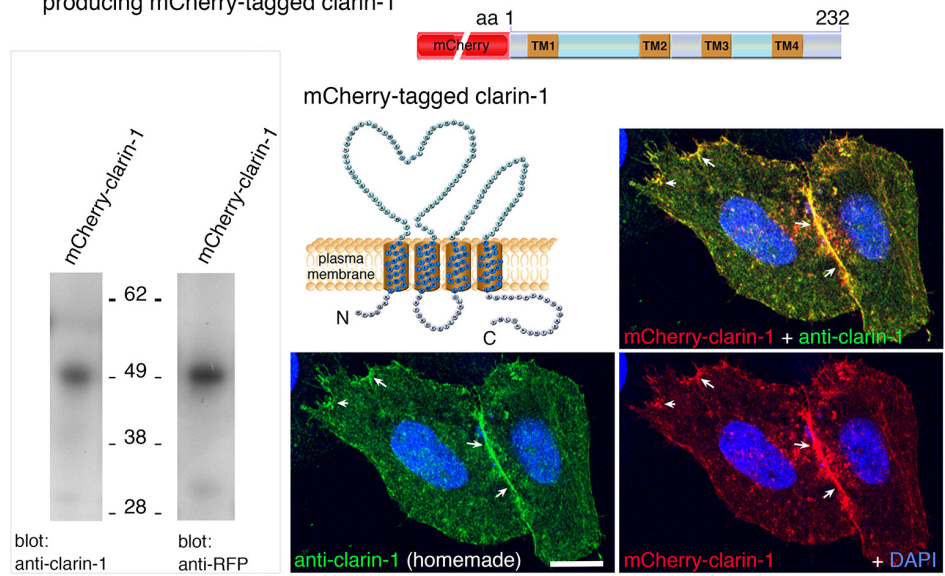


Supplemental Figure 4: Clarin-1 expression and test of anti-clarin-1 antibodies.

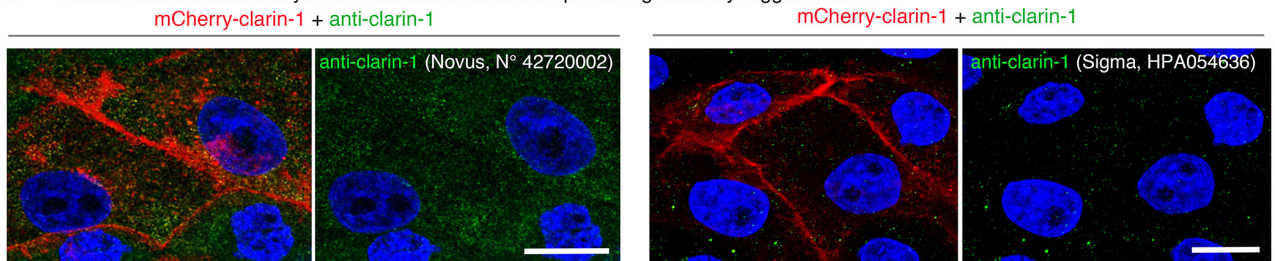
A Immunoblot analysis of the GST-tagged clarin-1 N-terminal fragment



B Immunoblot and immunofluorescence analysis of transfected HeLa cells producing mCherry-tagged clarin-1

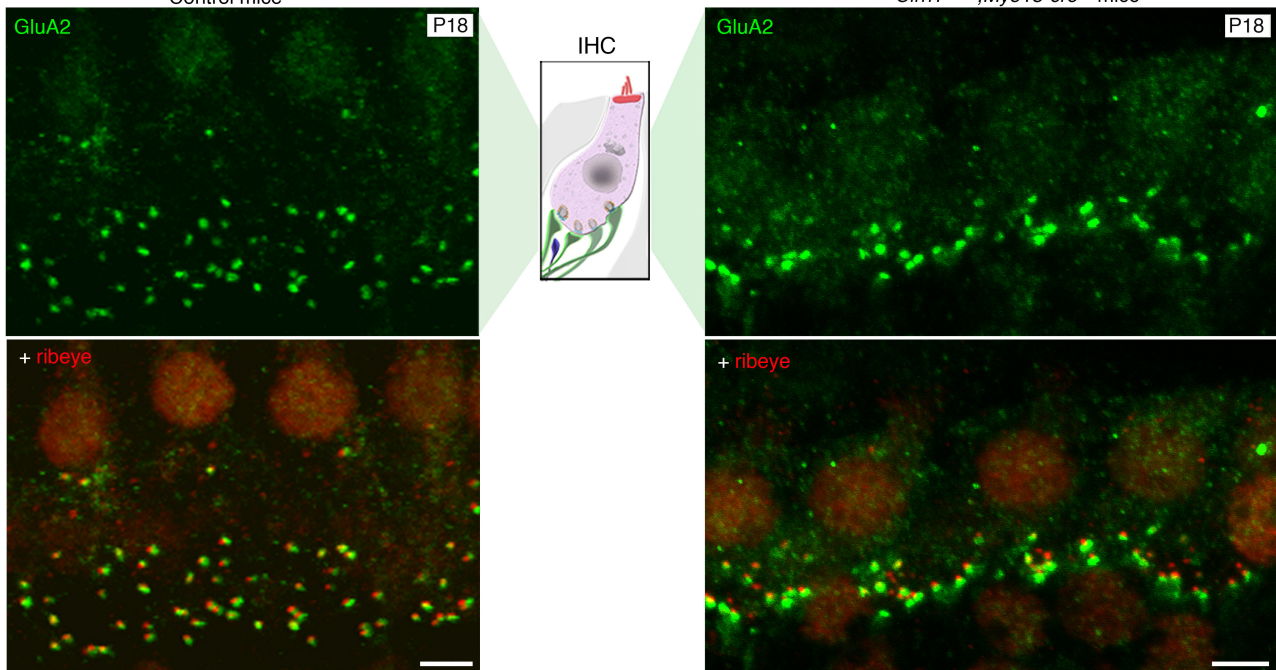


C Immunofluorescence analysis of transfected HeLa cells producing mCherry-tagged clarin-1

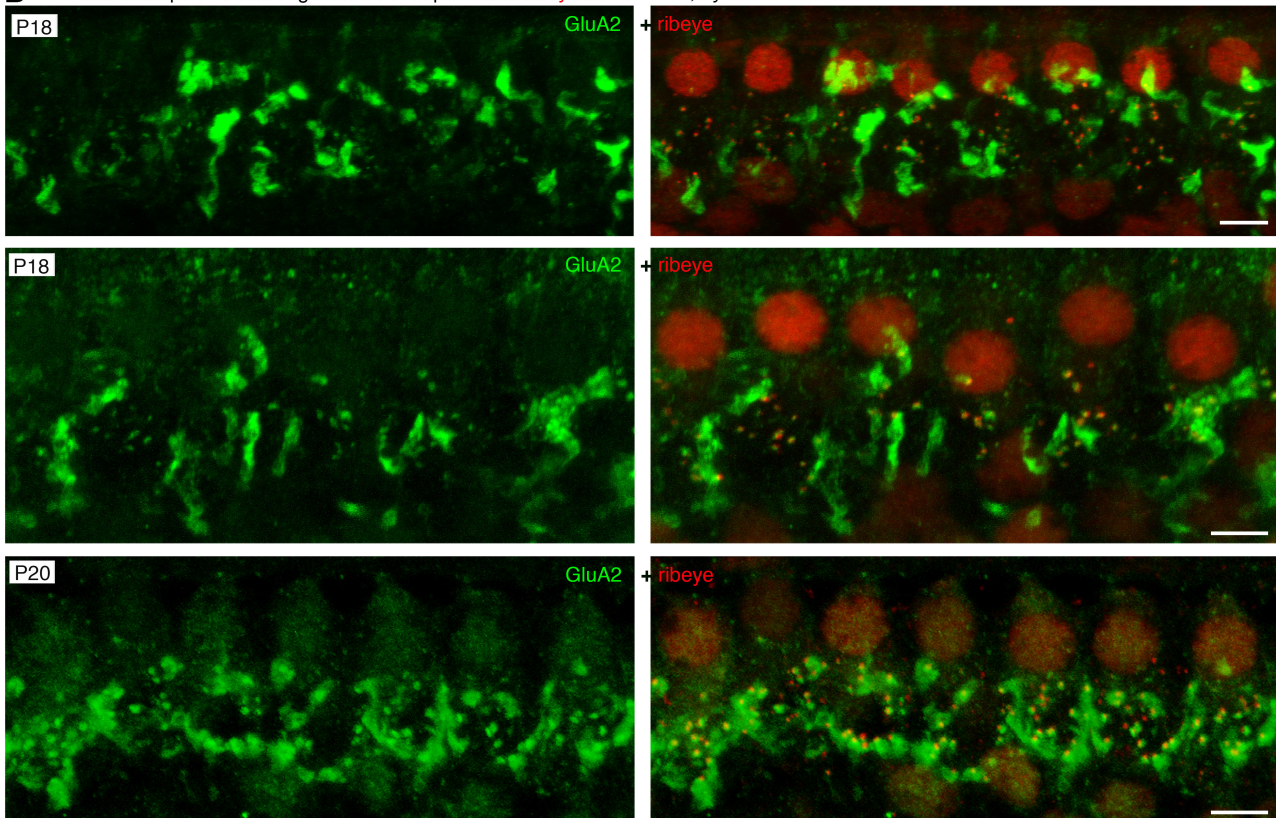


Supplemental Figure 5: Clarin-1 is required for the proper organization of the postsynaptic AMPA receptors GluA2/3 in *Clnr1^{ex4fl/fl}*, *Myo15-cre^{+/-}* mice.

A GluA2 glutamate receptors and ribeye in control and *Clnr1^{ex4fl/fl}*, *Myo15-cre^{+/-}* mice



B Other examples of GluA2 glutamate receptors and ribeye in *Clnr1^{ex4fl/fl}*, *Myo15-cre^{+/-}* mice



III- Supplemental Tables 1-3

Supplemental Table 1: Properties of Ca²⁺ currents in IHCs of control, *Cln1*^{ex4fl/fl}, *Myo15-cre*^{+/-}, and *Cln1*^{ex4-/-} mice

Ca²⁺-currents were activated using a depolarizing voltage-ramp protocol (1 mV/ms) from -90 to +30 mV. Currents were leak-subtracted on line, and voltage-error due to R_s was compensated. The activation curve was fitted with a Boltzman function from -50 to -5 mV to obtain the half-maximum voltage activation (V_{1/2}) and slope (S).

Supplemental Table 1: Properties of Ca ²⁺ currents in <i>Cln1</i> ^{ex4-/-} and <i>Cln1</i> ^{ex4fl/fl} , <i>Myo15-cre</i> ^{+/-} IHCs												
	<i>Cln1</i> ^{+/+} , <i>Cln1</i> ^{+/-}		<i>Cln1</i> ^{ex4-/-}		<i>Cln1</i> ^{ex4fl/fl}				<i>Cln1</i> ^{ex4fl/fl} , <i>Myo15-cre</i> ^{+/-}			
	P9 (n=15)	P13 (n=10)	P9 (n=13)	P13 (n=19)	P6 (n=7)	P9 (n=8)	P11 (n=15)	P18-P21 (n=8)	P6 (n=8)	P9 (n=8)	P11 (n=18)	P18-P21 (n=7)
<i>I</i>_{Ca²⁺} peak amplitude (pA)	240±12	147±8	235±10	225±10	189±29	315±38	185±9	161±11	194±17	356±53	292±14	250±20
<i>I</i>_{Ca²⁺} peak density (pA/pF)	23.6±0.9	13.4±0.8	25.3±1.3	23.3±1.0	20.3±3.2	33.2±4.0	16.7±0.8	13.1±0.9	20.08±1.8	35.6±5.3	28.4±1.3	28.1±2.2
Halfmax Voltage Activation V_{1/2} (mV)	-26.7±0.1	-27.5±0.2	-28.7±0.2	-29.6±0.2	-30.2±1.2	-29.8±0.3	28.4±0.2	-26.0±0.3	-28.9±0.9	-32.3±0.5	-31.6±0.2	-33.2±0.5
Boltzman slope S (pA/mV)	6.0±0.1	5.8±0.1	6.0±0.1	5.4±0.1	5.8±0.3	4.7±0.2	4.8±0.2	5.7±0.2	5.8±0.2	4.0±0.3	4.19±0.1	4.2±0.1

Supplemental Table 2: Summary characteristics of exocytosis in *Clnr1*^{ex4-/-} and *Clnr1*^{ex4fl/fl},*Myo15-cre*^{+/-} IHCs

RRP kinetics: exocytosis was evoked by voltage-steps from -80 mV to -10 mV with increasing duration from 10 to 100 ms. Data were fit with a single exponential. RRP Ca²⁺ efficiency: exocytosis was evoked by stepping the cells at different potentials from -80 mV to -10 mV in 10 mV increments, each step having a constant 100 ms duration. Data were fit with a power function as described in Figure 5.

Supplemental Table 2: Characteristics of exocytosis in <i>Clnr1</i> ^{ex4-/-} and <i>Clnr1</i> ^{ex4fl/fl} , <i>Myo15-cre</i> ^{+/-} IHCs										
	Exocytosis in <i>Clnr1</i> ^{ex4-/-}				Exocytosis in <i>Clnr1</i> ^{ex4fl/fl} , <i>Myo15-cre</i> ^{+/-}					
	<i>Clnr1</i> ^{+/+} , <i>Clnr1</i> ^{+/-}		<i>Clnr1</i> ^{ex4-/-}		<i>Clnr1</i> ^{ex4fl/fl}			<i>Clnr1</i> ^{ex4fl/fl} , <i>Myo15-cre</i> ^{+/-}		
	P9	P13	P9	P13	P9	P13	P18	P9	P13	P18
	RRP Kinetics EGTA 1 mM (τ in ms)	19±2 (n=11)	12.5±4.5 (n=6)	39±11 (n=6)	25±5* (n=9)	34±10 (n=7)	20±8 (n=11)	25±10 (n=12)	40±8 (n=15)	73±16* (n=16)
EGTA 5 mM (τ in ms)							33±18 (n=11)			205±32* (n=10)
RRP Ca²⁺ efficiency (fF/pA)	0.04 ± 0.02 (n= 11)	0.13 ± 0.01 (n= 6)	0.04 ± 0.01 (n= 4)	0.04 ± 0.01* (n=9)	0.06 ± 0.1 (n= 5)	0.16 ± 0.01 (n=10)	0.16 ± 0.01 (n=15)	0.05 ± 0.01 (n=15)	0.07 ±0.01* (n=11)	0.08 ± 0.01* (n=25)
N power fit	1.35±0.1	0.54±0.2	1.38±0.2	1.0±0.1	0.8±0.4	0.8±0.1	0.71±0.1	0.8±0.2	0.9±0.1	0.71±0.1

Supplemental Table 3: Properties of Ca²⁺ currents and exocytosis in *Cln1*^{ex4-/-}-AAV2/8-*Cln1* rescued IHCs. Ca²⁺-currents and exocytosis were recorded as described in Supplemental Tables 1 and 2.

Supplemental Table 3: Properties of Ca²⁺ currents in <i>Cln1</i>^{ex4-/-}-AAV2/8-<i>Cln1</i> rescued IHCs			
	Control <i>Cln1</i>^{+/+}, <i>Cln1</i>^{+/-} (AAV2/8-<i>Cln1</i>)	<i>Cln1</i>^{ex4-/-}	Rescued <i>Cln1</i>^{ex4-/-} (AAV2/8-<i>Cln1</i>)
	P15-P18 (n = 9)	P15-P18 (n = 9)	P15-P18 (n = 16)
<i>I</i>_{Ca²⁺} peak amplitude (pA)	175.7 ± 9.9	255.1 ± 23*	159.6 ± 12.3 (p = 0.39)
Half max voltage activation V_{1/2} (mV)	- 24.9 ± 1.3	- 30.8 ± 1.6*	- 22.9 ± 0.9 (p = 0.23)
Boltzman slope S (pA/mV)	5.87 ± 0.13	4.51 ± 0.15*	5.60 ± 0.12 (p = 0.16)

Characteristics of exocytosis in <i>Cln1</i>^{ex4-/-}-AAV2/8 rescue IHCs			
	Control <i>Cln1</i>^{+/+}, <i>Cln1</i>^{+/-} (AAV2/8-<i>Cln1</i>)	<i>Cln1</i>^{ex4-/-}	Rescued <i>Cln1</i>^{ex4-/-} (AAV2/8-<i>Cln1</i>)
	P15-P18 (n=9)	P15-P18 (n=9)	P15-P18 (n=16)
Kinetics: RRP exocytosis rate (linear fit over the first 40 ms) (pF/s)	0.37 ± 0.06	0.15 ± 0.03*	0.36 ± 0.05 (p = 0.9)
RRP Ca²⁺ efficiency (fF/pA)	0.17 ± 0.02	0.07 ± 0.01*	0.18 ± 0.01 (p = 0.8)

* Statistical difference with $p < 0.05$ (unpaired Student *t*-test) for *Cln1*^{ex4-/-} and *p* values in parenthesis for the rescue as compared to control.

IV- Supplemental Methods

Generation of clarin-1-deficient mice

To engineer clarin-1-deficient mice, we used the cre-lox system to delete *Clrn1* exon-4 (see Figure 1B,C). The *Clrn1*^{ex4fl/fl} mice carrying the LoxP sites on both alleles were used (these floxed mice are on a C57BL/6N genetic background). They are crossed (1 backcross in each case) with *PGK-cre*^{+/-} mice (mixed BALB/c & C57BL/6N inbred genetic backgrounds) to obtain a precocious and ubiquitous suppression of clarin-1 (*Clrn1*^{ex4-/-} mice: official nomenclature from Mouse Genome Informatics (MGI) symbol: *Clrn1*^{tm1.2Ugpa}, MGI accession ID:6099052, and with *Myo15-cre*^{+/-} mice (1, 2; these mice are on a C57BL/6N genetic background) to specifically target clarin-1 suppression to hair cells at postnatal stages (*Clrn1*^{ex4fl/fl}, *Myo15-cre*^{+/-} mice: *Clrn1*^{tm1.1Ugpa}, MGI accession ID:6099051).

RT-PCR for isoform specificity

For RT-PCR analyses, freshly dissected inner ears were collected from P15 wild-type mice. Organs of corti and inner hair cells (IHCs) were microdissected separately and quickly frozen in liquid nitrogen and stored at -80°C until processing. Total RNAs were isolated with TRIzol Reagent (Invitrogen) according to the manufacturer's instructions. Total RNA (100 ng) was reverse-transcribed with the SuperScript III One-Step RT-PCR system (Invitrogen) as described by the manufacturer using various isoform specific primers: For isoform 1 containing exon-1,2,3,4 the forward primer was AAGGCCTTCCGGTTCTCATCAAG; For isoform 2 containing exon-1,3,4 the forward primer was CCTTCCGGTTCTCATCTTCCC); For isoform 3 containing exon-1,4 the forward primer was CCTTCCGGTTCTCATGCTCC); the reverse primer common to all isoforms (in exon-4) was AAATCTGAAGCTACATTAGTGGTCTCTG.

The final PCR products were electrophoresed on 2.0% agarose gels containing EtBr along with DNA markers. Reverse transcription negative controls, containing all RT-PCR reagents except the reverse transcriptase (-RT) were used where no amplification was observed. As a positive control (see Figure 1B), we used primers derived against mouse *Myo7a*: 6375s (CACCTGATGACTGGAAAC) and 6715as (ATCATCCATTTT GTATCCC).

Expression vectors, antibodies and protein-protein interactions

The mouse cDNA encoding full-length clarin-1 (NP_700434.1), obtained from a mouse inner ear cDNA library, was used to produce two clarin-1 fragments: *Clrn1*-N (amino acids (aa) 1-136) and *Clrn1*-C (aa 121-232). All PCR-amplified fragments were inserted into pCR2.1-TOPO (Invitrogen), and their sequences were checked before transfer to the appropriate vectors, *i.e.* mCherry and pECFP (Clontech), pCMV-tag3B (Myc tag, Stratagene), and pcDNA3 (No tag or Flag tag, Invitrogen) for

transfection experiments, or pGEX-//2 (GST tag, Amersham) for protein production. The cDNAs encoding the rat Cav1.3 α_1 (aa 1-2203, NP_058994.1) and Cav1.3 β_2 (aa 2-604, NP_4466303.1) subunits (kindly provided by S. Seino, Kobe University Graduate School of Medicine, Japan), and the α interaction domain of Cav α_1 (AID, aa 406-576, NP_058994.1) were also used for in vitro binding experiments.

We used mouse Clrn1-N (aa 1-136) to generate rabbit anti-clarin-1 polyclonal antibodies. Immunoblot analyses using bacterial cell lysates expressing Clrn1-N confirmed the specificity of the anti-clarin-1 purified antibody (Supplemental Figure 4A,B). Purified anti-clarin1 homemade antibodies, but not the commercial Novus or Sigma antibodies, did detect mCherry-tagged clarin-1 in transfected cells (Supplementary Figure 4B). However, repeated attempts to detect endogenous clarin-1 in the mouse auditory sensory organ at different postnatal stages, under various conditions of fixation and antigen-retrieval, were unsuccessful. Anti-myosin VIIa, anti-cadherin-23, anti-sans, anti-harmonin, and anti-protocadherin-15 antibodies (3) were used for the detection of USH proteins. The following primary antibodies were also used: rabbit anti-stereocilin (4), mouse anti-otoferlin (Abcam, Paris, France; cat # ab53233), mouse (1:200; C1- sc-17805; E12 sc-17759) and rabbit (Santa Cruz, USA; cat # SC-5966) anti-CtBP2 antibodies (1:200) to detect the ribbon protein ribeye, rabbit anti-Cav1.3 (1:80; Alomone Labs, cat # ACC-005), rabbit anti-GluA2/3 (1:200; Millipore, cat # AB1506), rabbit anti-GFP (Invitrogen-ThermoFisher Scientific, cat # A-11122,), rabbit anti-RFP (Rockland, cat # N° 600-104-379), mouse anti-myc (Santa Cruz, USA, cat # sc-40), mouse anti-Flag2 tag (Sigma Aldrich, cat # F3165), and chicken anti-neurofilament (NF200, Millipore, cat # AB5539) antibodies. The secondary antibodies (Invitrogen-ThermoFisher Scientific) were Alexa Fluor 488-conjugated goat anti-rabbit (cat # A-11034), Alexa Fluor 488-conjugated goat anti-mouse (cat # A32723), Alexa Fluor 488-conjugated donkey anti-goat (cat # A-21081), Cy3-conjugated anti-mouse (cat # A10521), and Cy3-conjugated anti-rabbit (cat # A10520), and Alexa 488-conjugated goat anti-chicken (cat # A-11039) antibodies.

Immunofluorescence and electron microscopy analyses

Inner ears were fixed by incubation in 4% paraformaldehyde in phosphate-buffered saline (PBS), pH 7.4, at 4°C for 1-2 hours, except for the detection of Cav1.3, for which cochleae were perfused and fixed with 100 % cold methanol at -20°C for 30 min.

For immunofluorescence analyses, samples (microdissected auditory sensory organs) were incubated in PBS supplemented with 30% normal horse serum for 1 hour at room temperature. They were then washed three times in PBS and incubated at 4°C overnight with the primary antibodies, in PBS supplemented with 5% horse serum and 0.1% Triton X-100. The samples were rinsed in PBS, incubated for 1-2 hours with the appropriate secondary antibodies, and counterstained with DAPI

nuclear stain (Sigma-Aldrich, cat # 28718-90-3) and/or phalloidin conjugated with either TRITC (Sigma-Aldrich, cat # P1951) or Alexa546 (Invitrogen-ThermoFisher Scientific, cat # A22283) to visualize actin filaments. Images were acquired with Leica SP8 (Leica, Bordeaux Imaging Center) or Zeiss LSM700 (Zeiss, Pasteur Institute) confocal laser scanning microscopes (LSMs) equipped with a plan Apo 63x NA 1.4 oil immersion objective lens, and they were processed with Photoshop CS6 as previously described (3). Ribbon synapses and/or Cav1.3-immunoreactive spots were counted as described (5), using 3D reconstructions of all confocal z-stacks, and focusing on ribbons juxtaposed with the postsynaptic GluA2/3 immunoreactive spots. To obtain a count per IHC (mean \pm SEM), the number of ribbons counted was divided by the number of IHCs analyzed. All comparisons between control and clarin-1-deficient mice were processed under the same conditions of preparation, acquisition and analysis. For area quantification, z-stack confocal images (0.25 μ m) were treated for deconvolution with AutoQuant X2 (blind deconvolution), and 3D construction was then varied out with Imaris software (Bitplane AG).

For ultrastructural analyses, cochleae were perfused with 4% paraformaldehyde and 2% glutaraldehyde in PBS at pH 7.4 and immersed in the same fixative solution for 2 hours. They were then post-fixed by overnight incubation in 1% osmium tetroxide at 4°C, dehydrated in graded series of acetone concentrations, and embedded in Spurr's low-viscosity epoxy resin hardened at 70°C. Ultrathin sections were cut and transferred to formvar-coated single-slot grids, stained with uranyl acetate and lead citrate, and examined under a Jeol1200EX electron microscope (Pasteur, Imagopole). A minimum of 3 mice were used for each type of mutant and control mice for EM analyses.

For scanning electron microscopy, inner ears were fixed by incubation in 2.5% glutaraldehyde in 0.1 M phosphate buffer (pH 7.3) for 2 hours at room temperature. The samples were washed several times in the buffer alone, and cochlear sensory epithelia were carefully dissected and processed by the osmium tetroxide/thiocarbohydrazide (OTOTO) method, as previously described (6). Samples were analyzed by field emission scanning electron microscopy (Jeol JSM6700F operating at 5 kV). Images were obtained with a charge-coupled device camera (SIS Megaview3; Surface Imaging Systems), acquired by analySIS (Soft Imaging System), and processed with Photoshop CS6.

Quantification of neuron density in the cochlear ganglia

The method used was same as previously described by Kaur *et. al* (7) with slight modifications. Briefly inner ears were dissected in phosphate-buffered saline (PBS) and fixed by immersion in 4% paraformaldehyde (PFA) in PBS for 2 hours at 4°C. The samples were decalcified by incubation in 10% EDTA in PBS, pH 7.4, for 4 days at 4°C, fixed again in 4% PFA in PBS for 1 hour, rinsed twice in PBS for 10 minutes each, and immersed in 20% sucrose in PBS for 12 hours. They were embedded in Tissue Freezing Medium (Sakura finetek, USA) and frozen. Cryostat sections (20 μ m thick) were

used for immunofluorescence as described previously (8). Cryosectioned tissues were rinsed with PBS and incubated at room temperature for 2 h in blocking solution (10% normal horse serum in 0.3% Triton X-100 in PBS). Sections were then incubated overnight at room temperature with anti-parvalbumin antibody (1:200; Sigma-Aldrich, cat # SAB4200545) to label spiral ganglion cell bodies. Specimens were then rinsed 5x in PBS and incubated for 2 h in secondary antibody (1:500; Atto 488 anti-mouse IgG, Sigma-Aldrich, cat # 62197) followed by incubation with DAPI (1:10000). Fluorescence imaging was performed using a Zeiss LSM 700 confocal microscope. Z-series images at 0.3 μm intervals were obtained using a 20x objective. Image processing and quantitative analysis were performed using Image J software. To assess the numbers of spiral ganglion cell bodies, parvalbumin labeled SGNs within Rosenthal's canal were counted from the maximum intensity projections of each section. Cell bodies were counted from 5-6 sections per cochlea and were normalized to the cross-sectional area of Rosenthal's canal in the basal turn and averaged and reported as SGN density (cells per 1000 μm^2). Statistical comparisons were made using one-way ANOVA's with post hoc Holm-Sidak tests.

Protein-protein binding experiments

Equal amounts of fusion proteins were used for *in vitro* binding assays as previously described (8, 9). Fusion proteins were produced in BL21(DE3)codonPlus-RP *E. coli* cells and HEK293 cells (ATCC), used as bacterial and eukaryotic expression systems, respectively. Transfections of HEK293 cells were performed at 90-95% confluence, in the presence of Lipofectamine 2000 reagent (Invitrogen), in accordance with the manufacturer's recommendation, as previously described (8, 9). Tagged fusion proteins were purified with the appropriate resin for the tag used: GST (glutathione Sepharose 4B, GE Healthcare), Flag, Myc, or ECFP (MiltenyBiotec SAS, France). Briefly, for clarin-1-Cav β_2 interaction, a bacterial lysate containing GST alone or GST-tagged Cln1-N was incubated with pre-equilibrated glutathione-Sepharose beads at 4°C for 90 minutes. The beads were washed three times in the binding buffer (5% glycerol, 5 mM MgCl₂ and 0.1% Triton X-100 in PBS) supplemented with a protease inhibitor cocktail (Roche), and then incubated with a cell lysate of HEK293 cells producing CFP-tagged Cav β_2 , on a rotating wheel at 4°C for 3 hours. The beads were then washed four times in the binding buffer supplemented with 150 mMNaCl. Bound proteins were suspended in 30 μl of 2x concentrated SDS sample buffer and submitted to western blot analysis. Horseradish peroxidase (HRP)-conjugated goat anti-rabbit (Jackson ImmunoResearch, cat #211-032-171) or anti-mouse (Jackson ImmunoResearch, cat # 115-035-174) antibodies and the ECL chemiluminescence system (Pierce, Rockford, cat # 32209) were used for detection.

For immunoprecipitation, protein extracts of HEK293 cells were prepared by using 500 μl of immunoprecipitation buffer (150 mMNaCl, 50 mMTris-HCl, pH 7.5, 500 μM EDTA, 100

μM EGTA, 0.1% SDS, 1% Triton-X100, and 1% sodium deoxycholate), supplemented with an EDTA-free cocktail of protease inhibitors (Roche). The soluble fraction was incubated for 6 hours with the anti-Flag, the pre-immune serum, or the immunoprecipitation buffer alone, then with 50 μl of pre-equilibrated protein G beads (Pierce) at 4°C overnight. The beads were washed three times in the immunoprecipitation buffer, and the bound proteins were submitted to western blot analysis (see above).

Each type of binding assay experiment is performed at least in triplicate. A positive interaction is considered significant with respect to differences with negative controls (e.g. GST alone, Flag beads alone, CFP alone, or CFP-tagged rab-11 alone) used in the same conditions. Densitometric quantification of the bands obtained was performed using ImageJ software and student's *t*-test was performed to evaluate statistical significance. A *P* value of < 0.05 was considered to be significant for data acquired in arbitrary density units.

***In vivo* auditory tests**

Auditory brainstem responses (ABRs), compound action potentials (CAPs), and distortion product otoacoustic emissions (DPOAEs) were recorded in anesthetized mice, and the results were analyzed as described (6, 10). Animals were anesthetized with a mixture of ketamine (150 mg/kg) and levomepromazine (2 mg/kg), with additional half doses given every 30 min. The body temperature of the animals was maintained at 37°C with a regulated heating blanket. For CAP measurements, a Teflon-coated silver-wire electrode was surgically inserted into the round-window niche, with the negative and ground electrodes positioned subcutaneously in the skull and neck regions. The electrocochleogram was collected with a Grass preamplifier (gain $\times 10,000$) and numerically averaged (CED 1401+ processor) in synchrony with the stimulus ($\times 32$). For ABR recordings, three steel electrodes were inserted (negative and ground as for CAP measurements, with a positive electrode inserted in the mastoid region). The electroencephalogram was collected by the preamplifier with a $\times 100,000$ gain, and numerically averaged over 256 epochs.

For both ABR and CAP recordings, the sound stimuli used were tone-bursts produced by a Wavetek-70 arbitrary waveform generator (2-period rise and decay times, 16-period plateau) and sent to a Radioshack tweeter (40-1376, 8 Ω – 70 W) connected to a conical tip. Tone-burst frequencies were in the range of 5 to 40 kHz. At each frequency, the threshold-searching procedure could apply sound intensities from 10 to 115 dB SPL in 2 to 5 dB steps. ABR and CAP thresholds were defined as the sound level producing the smallest detectable wave, shown to be reproducible to sound levels within 2 dB.

For DPOAE measurements, f_1 and f_2 stimuli were applied through different earphones and tubing to avoid nonlinear interactions on earphone membranes. Only the cubic difference tone at $2f_1$ -

f_2 , the most prominent one from the ear was detected. This DPOAE comes mostly from the site of maximum overlap between basilar membrane vibrations to f_1 and f_2 , close to the site tuned to f_2 . We therefore plotted the DPOAE threshold against f_2 . The f_2 frequency was swept from 5 to 32 kHz in $1/8^{\text{th}}$ octave steps, with f_1 chosen such that the frequency ratio f_2/f_1 was 1.20. The intensities of the two tonal stimuli at f_1 and f_2 were the same, from 20 to 80 dB SPL in 5 dB steps. The DPOAE threshold was defined as the weakest stimulus producing a DPOAE significantly above the background noise, estimated from the spectral lines closest to $2f_1-f_2$ in the 0.5 s sound samples collected in the ear canal.

For EEBR recordings, the eighth cranial nerve was stimulated electrically with a silver electrode placed in the round-window niche and excited by biphasic electrical impulses (neutral electrode in neck muscles; peak amplitude of electrical stimulus about 0.5 V; duration of the positive and negative phases 150 μ s). EEBRs were extracted with the same setup as for ABRs, as previously described (6).

Hair cell electrophysiology

All IHC recordings were performed in the 20–40% normalized distance from the apex, an area coding for frequencies ranging from 8 to 16 kHz. For IHC electrophysiological recordings, mouse organs of Corti, at different stages of postnatal development, were bathed at room temperature (22–24°C) in an extracellular solution, with the following composition: 135 mM NaCl, 5.8 mM KCl, 5 mM CaCl_2 , 0.9 mM MgCl_2 , 0.7 mM NaH_2PO_4 , 5.6 mM glucose, 2 mM Na-pyruvate, 10 mM HEPES, 250 nM apamin, 0.5 μ M XE-991, pH 7.4. The Ca^{2+} currents were recorded in the whole-cell voltage-clamp configuration, using 3–5 M Ω resistance pipettes with an EPC 10 amplifier and Patchmaster software (HekaElectronik, Lambrecht/Pfalz, Germany). The intracellular recording solution had the following composition: 145 mM CsCl, 1 mM MgCl_2 , 5 mM HEPES, 1 mM EGTA, 20 mM TEA, 2 mM ATP, 0.3 mM GTP, pH 7.4. Only recordings with a holding current of less than 50 pA at -80 mV were retained for analysis. Real-time changes in membrane capacitance (ΔC_m) were recorded with the software locking amplifier of Patchmaster. A 2 kHz sine wave of 10 mV was applied to the cells from a holding potential of -80 mV. Capacitance (C_m) signals were low-pass filtered at 80 to 100 Hz. Changes in membrane capacitance were measured 0.05–0.5 s after the end of the depolarizing pulse and averaged over a period of 0.3–20 s. Membrane and series resistance (R_m and R_s) values were monitored during the course of the experiment. Only recordings with stable R_m and R_s were considered for further analysis. R_s values averaged 8.9 ± 0.2 M Ω ($n = 221$; mean \pm SEM). The seal resistance was typically 5–20 G Ω .

To trigger a fast increase in intracellular Ca^{2+} concentration from the caged Ca^{2+} chelator DM-nitrophen (Interchim, France), we used brief flashes from a UV LED light source (Mic-LED 365,

128mW, Prizmatix, Givat Shmuel, Israel). The UV LED was directly connected to the epillumination port at the rear of our upright Nikon FN1 microscope and illumination was focalized through the 60X objective (CFI Fluor 60X W NIR, WD = 2.0 mm, NA=1). Hair cells were loaded with in mM, CsCl 145; HEPES 5; TEA 20; DM-nitrophen 10; CaCl₂ 10. The uncaging protocol increased the intracellular Ca²⁺ concentration above 20 μM (11). Sample C_m acquisition was done at 1 kHz.

Gene transfer through the cochlear round window membrane

A recombinant adeno-associated virus (AAV) carrying the mouse *Cln1* followed by an IRES-GFP sequence (AAV2/8-*Cln1*-IRES-GFP) was microinjected through the round window membrane on P1–P3 anesthetized mice. The virus was packaged and titrated by Penn Medicine Vector Core (University of Pennsylvania School of Medicine). Microinjections were performed on the left ear as described by (12). Briefly, the bulla was exposed after a dorsal incision, and a hole was made in the bulla large enough to allow access to the round window membrane. A fixed amount (2 μl) of a solution containing AAV2/8-*Cln1*-IRES-GFP (6×10^{12} vg/ml) was injected gently over 1 to 2 min period, after which the round window membrane was sealed with adipose tissue, and the bulla with was sealed with adhesive tape (3M Vetbond).

For quantification of *in vivo* injections of AAV2/8-*Cln1*-IRES-GFP, we captured high-magnification images along the cochlea at exactly the same distance from the base for all cochleas. Then, in each case, we manually counted all visible inner and outer hair cells and determined the percentage of GFP-positive cells.

Statistical analysis

For *in vivo* recordings (data expressed as mean ± SD or SEM, as indicated), statistical significance of the differences observed was tested with Student's *t*-test, two-way analysis of variance coupled to the Bonferroni post-hoc test (2-way ANOVA) or two-tailed unpaired *t*-test with Welch's correction using the Prism software (GraphPad, La Jolla, CA). For *ex-vivo* recordings, the data (expressed as mean ± SEM) were analyzed with Origin (Microcal, Northampton, MA) and Igor software (Wavemetrics, Portland, OR). Statistical significances are indicated on the figures. (ns), (*), (**), and (***) denote non-significant ($P > 0.05$), $P < 0.05$, $P < 0.01$, and $P < 0.001$, respectively.

Study approval

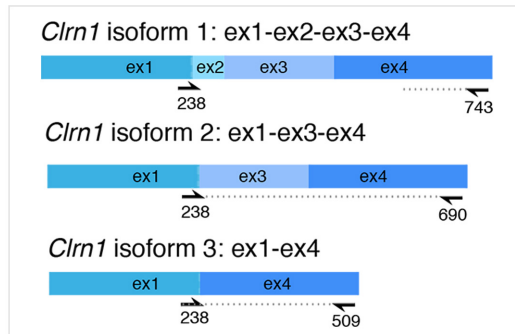
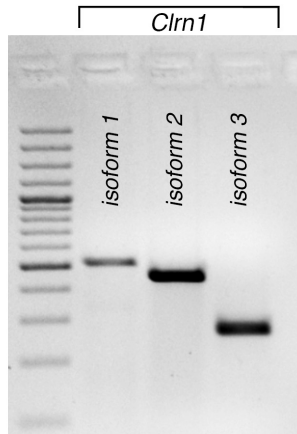
All the experiments on mice were carried out according to protocols approved by the Animal Use Committees of INSERM, University of Bordeaux (CEEA50) and Institut Pasteur (CETEA-2014-0032).

V- References

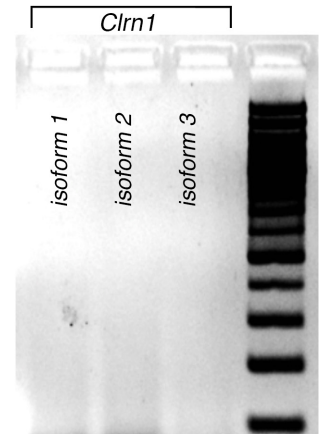
1. Caberlotto E, Michel V, Foucher I, Bahloul A, Goodyear RJ, Pepermans E, Michalski N, Perfettini I, Alegria-Prevot O, Chardenoux S, et al. Usher type 1G protein sans is a critical component of the tip-link complex, a structure controlling actin polymerization in stereocilia. *Proc. Natl Acad. Sci. USA*. 2011;108(14):5825-5830.
2. Pepermans E, Michel V, Goodyear R, Bonnet C, Abdi S, Dupont T, Gherbi S, Holder M, Makrelouf M, Hardelin JP, et al. The CD2 isoform of protocadherin-15 is an essential component of the tip-link complex in mature auditory hair cells. *EMBO Mol. Med*. 2014;6(7):984-992.
3. Sahly I, Dufour E, Schietroma C, Michel V, Bahloul A, Perfettini I, Pepermans E, Estivalet A, Carette D, Aghaie A, et al. Localization of Usher 1 proteins to the photoreceptor calyceal processes, which are absent from mice. *J. Cell Biol*. 2012;199(2):381-399.
4. Verpy E, Weil D, Leibovici M, Goodyear RJ, Hamard G, Houdon C, Lefevre GM, Hardelin JP, Richardson GP, Avan P, et al. Stereocilin-deficient mice reveal the origin of cochlear waveform distortions. *Nature*. 2008;456(7219):255-8.
5. Vincent PF, Bouleau Y, Safieddine S, Petit C, and Dulon D. Exocytotic machineries of vestibular type I and cochlear ribbon synapses display similar intrinsic otoferlin-dependent Ca^{2+} sensitivity but a different coupling to Ca^{2+} channels. *J. Neurosci*. 2014;34(33):10853-10869.
6. Kamiya K, Michel V, Giraudet F, Riederer B, Foucher I, Papal S, Perfettini I, Le Gal S, Verpy E, Xia W, et al. An unusually powerful mode of low-frequency sound interference due to defective hair bundles of the auditory outer hair cells. *Proc. Natl Acad. Sci. USA*. 2014;111(25):9307-9312.
7. Kaur T, Zamani D, Tong L, Rubel EW, Ohlemiller KK, Hirose K, and Warchol ME. Fractalkine Signaling Regulates Macrophage Recruitment into the Cochlea and Promotes the Survival of Spiral Ganglion Neurons after Selective Hair Cell Lesion. *J. Neurosci*. 2015;35(45):15050-15061.
8. Papal S, Cortese M, Legendre K, Soroush N, Dragavon J, Sahly I, Shorte S, Wolfrum U, Petit C, and El-Amraoui A. The giant spectrin betaV couples the molecular motors to phototransduction and Usher syndrome type I proteins along their trafficking route. *Hum Mol Genet*. 2013;22(18):3773-88.
9. Legendre K, Safieddine S, Kussel-Andermann P, Petit C, and El-Amraoui A. α II/ β V spectrin bridges the plasma membrane and cortical lattice in the lateral wall of auditory outer hair cells. *J. Cell Sci*. 2008;121:3347-56.
10. Le Calvez S, Avan P, Gilain L, and Romand R. CD1 hearing-impaired mice. I: Distortion product otoacoustic emission levels, cochlear function and morphology. *Hear. Res*. 1998;120(1-2):37-50.
11. Vincent PF, Bouleau Y, Petit C, and Dulon D. A synaptic F-actin network controls otoferlin-dependent exocytosis in auditory inner hair cells. *Elife*. 2015;4:e10988
12. Emptoz A, Michel V, Lelli A, Akil O, Boutet de Monvel J, Lahlou G, Meyer A, Dupont T, Nouaille S, Ey E, et al. Local gene therapy durably restores vestibular function in a mouse model of Usher syndrome type 1G. *Proc. Natl Acad. Sci*. 2017;114(36):9695-9700.

Expression of *Cln1* splice isoforms (1 to 3) in P15 and P30 mouse inner ears

RT-PCR on organs of Corti from P15 wild-type mice

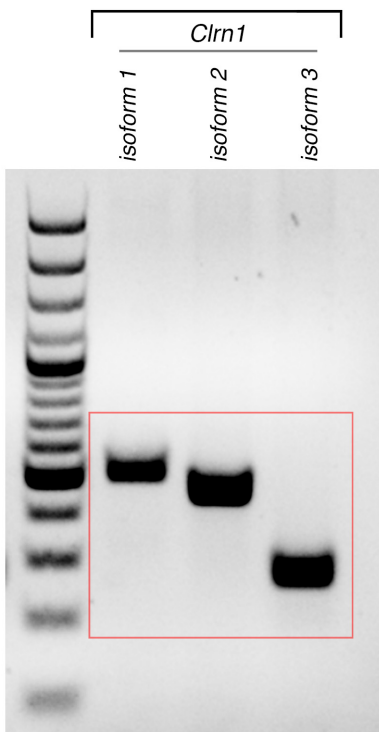


RT-PCR on isolated hair cells from P15 *Cln1*^{ex4fl/fl}, *Myo15-cre*^{+/-} mice

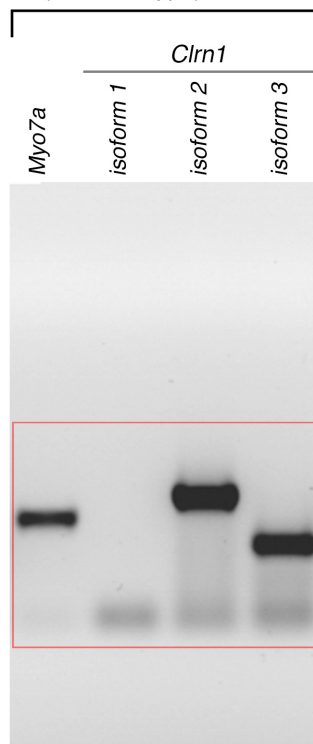


Boxed areas in red are the regions used in Figure 1B

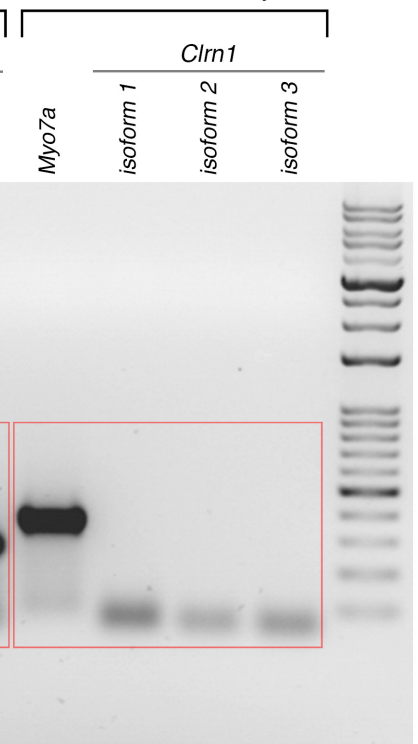
RT-PCR on organs of Corti from P30 wild-type mice



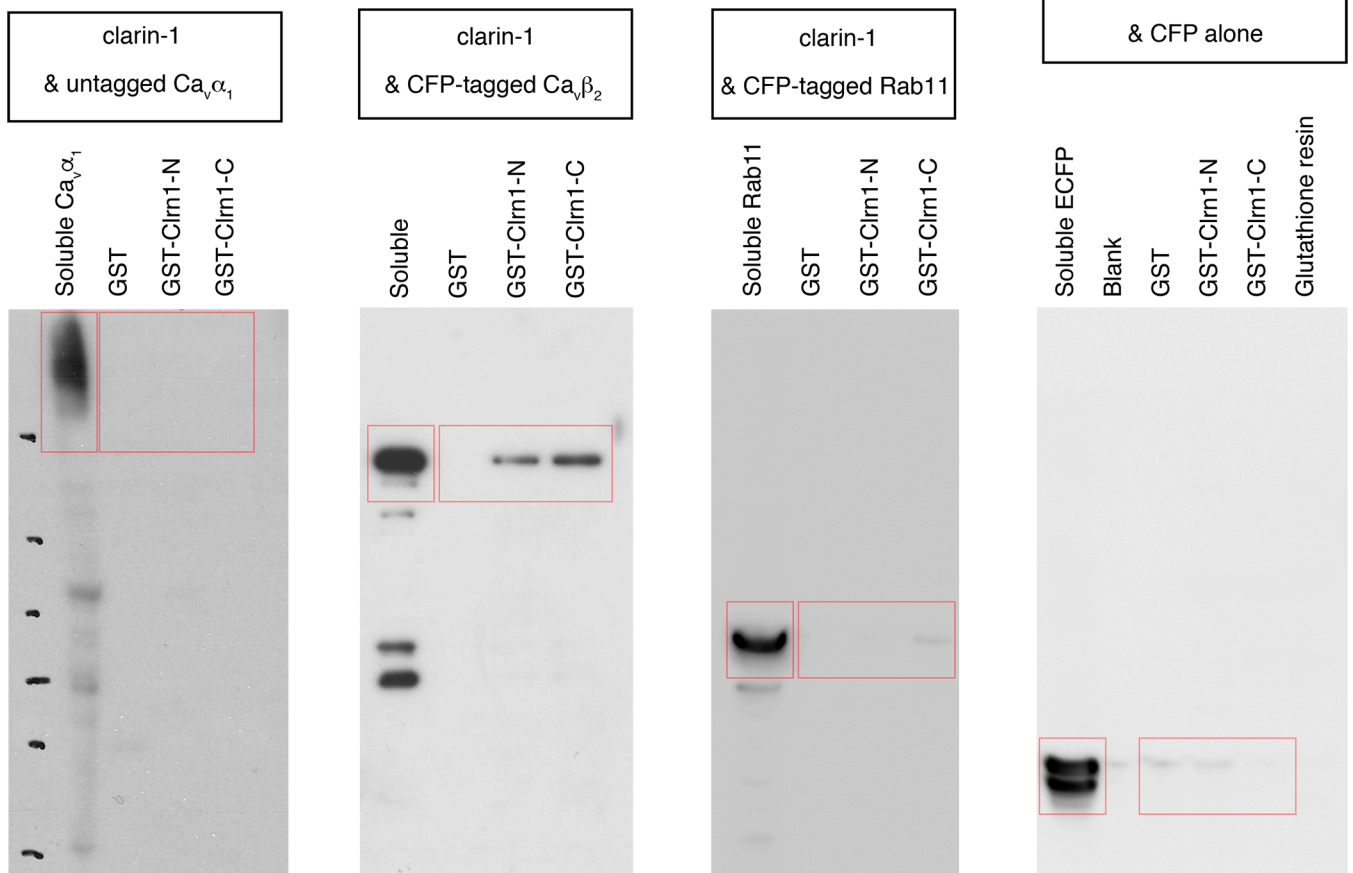
RT-PCR on isolated hair cells (P30 wild-type)



RT-PCR on isolated hair cells P30 *Cln1*^{ex4fl/fl}, *Myo15-cre*^{+/-}

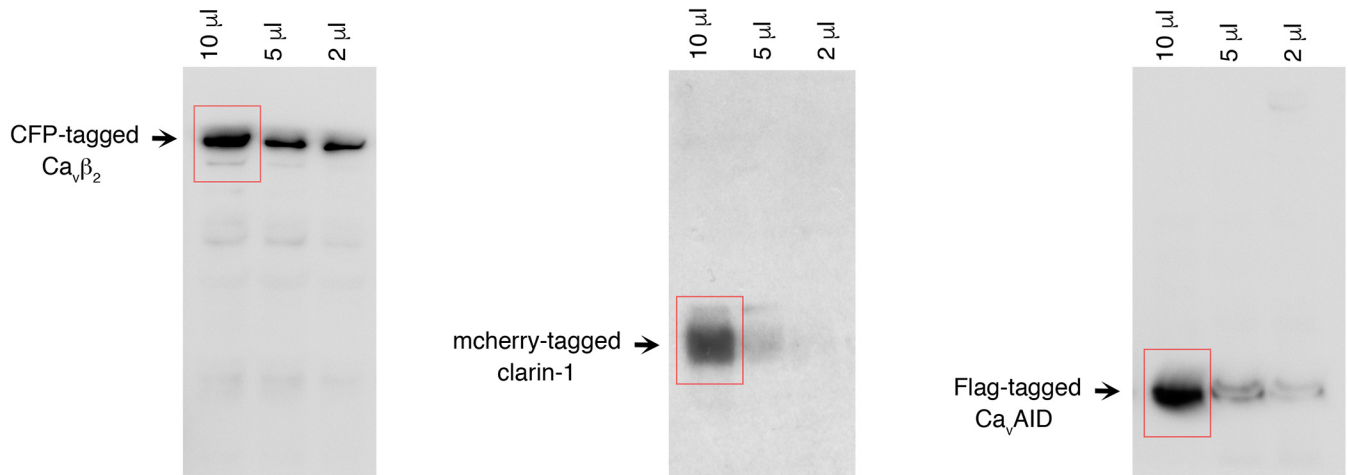


Boxed areas in red are the region used in Figure 11A

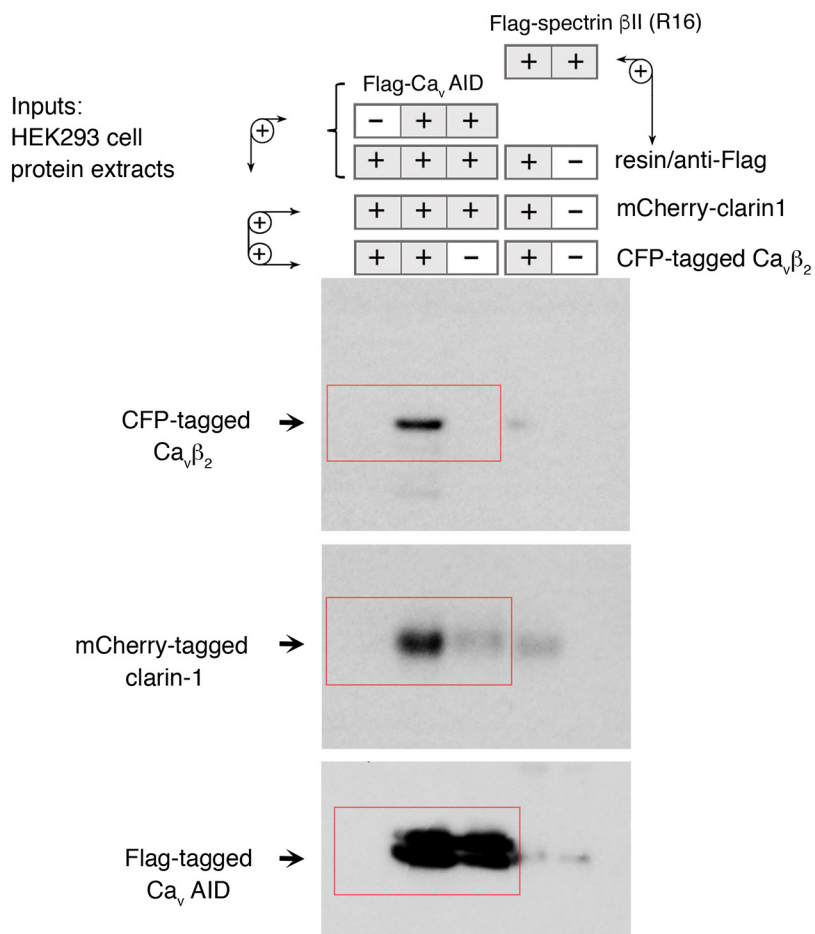


Boxed areas in red are the regions used in Figure 11C

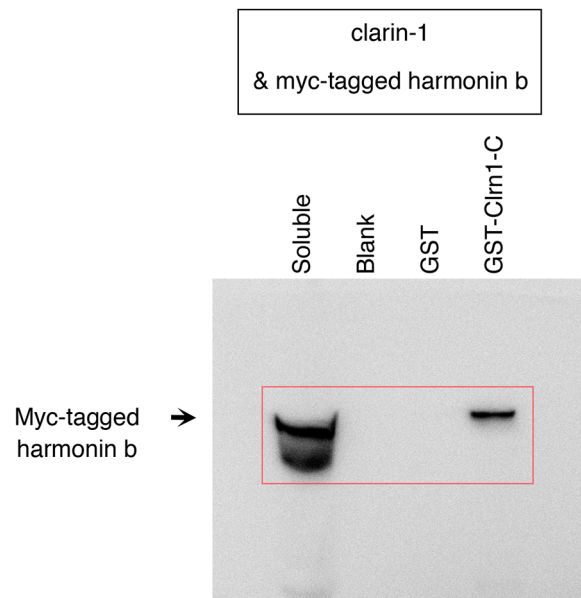
A Immunoblots to test soluble fractions of produced CFP-tagged $Ca_v\beta_2$, mCherry-tagged clarin-1 & Flag-tagged Ca_vAID



B Immunoblots of bound proteins to anti-Flag resin alone or conjugated to Flag-tagged Ca_vAID

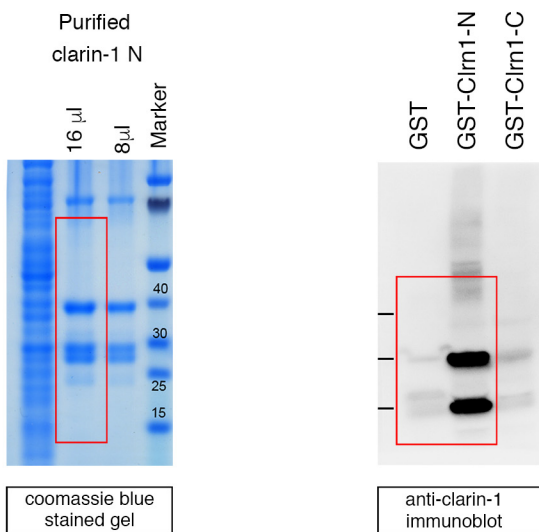


The boxed area in red is the region used in Figure 1E



Boxed areas in red are the regions used in supplemental Figure 4A,B

Test of the anti-clarin-1 antibody on GST-tagged clarin-1 N produced in bacteria



Test of the anti-clarin-1 antibody on mCherry-tagged clarin-1 produced in HEK293 cells

